Water vapor uptake into hygroscopic lithium bromide desiccant droplets: Mechanisms of droplet growth and spreading

View Article Online
DOI: 10.1039/C8CP04504F

Water vapor uptake into hygroscopic lithium bromide desiccant droplets: Mechanisms of droplet growth and spreading

Zhenying Wang[ab], Daniel Orejon[†ab], Khellil Sefiane[c], Yasuyuki Takata[‡ab]

a International Institute for Carbon-Neutral Energy Research (WPI-I^{2}CNER), Kyushu University, Fukuoka 819-0395, Japan

b Department of Mechanical Engineering, Thermofluid Physics Laboratory, Kyushu University, Fukuoka 819-0395, Japan

c School of Engineering, Institute for Multiscale Thermofluids, University of Edinburgh, King's Buildings, Mayfield Road, Edinburgh EH9 3JL, United Kingdom

Corresponding author: † orejon.daniel@heat.mech.kyushu-u.ac.jp; ‡ takata@mech.kyushu-u.ac.jp.

ABSTRACT

The study of vapor absorption into liquid desiccant droplets is of general relevance to a better understanding and description of vapor absorption phenomena occurring at the macroscale as well as for practical optimization of dehumidification and refrigeration processes. Hence, in the present work, we provide the first systematic experimental study on the fundamentals of vapor absorption into liquid desiccant at the droplet scale, which initiates a novel avenue for the research of hygroscopic droplet growth. More specifically we address the behavior of lithium bromide-water droplets on hydrophobic PTFE and hydrophilic glass substrates under controlled ambient conditions. Driven by the vapor pressure difference between the ambient air and the droplet interface, desiccant droplets absorb water vapor and increase in volume. To provide further insights on the vapor absorption process, the evolution of the droplet profile is recorded using optical imaging and relevant profile characteristics are extracted. Results show that, even though the final expansion ratio of droplet volume is only function of relative humidity, the dynamics of contact line and the absorption rate are found to differ greatly when comparing data with varying substrate wettability. Droplets on hydrophilic substrates show higher absorption kinetics and reach equilibrium with the ambient much faster than those on hydrophobic substrates. This is attributed to the absorption process being controlled by solute diffusion on the droplet side and to the shorter characteristic length for the solute diffusion on hydrophilic substrates. Moreover, the apparent droplet spreading process on hydrophilic substrates when compared to hydrophobic ones is explained based on a force balance analysis near the triple contact line, by the change of liquid-vapor surface tension due to the increase in water concentration, and assuming a development of a precursor film.

Keywords: liquid desiccant, spreading, surface wettability, droplet dynamics, vapor absorption

View Article Online
DOI: 10.1039/C8CP04504F

1. INTRODUCTION

Droplet evaporation is a widely observed phenomenon in nature, and has been applied in several industrial and biological fields from ink-jet printing [1] and thin film coating [2,3], to DNA stretching and disease diagnosis [4]. In recent years, an increasing number of investigations have been carried out on the effect of ambient pressure [5,6], ambient temperature and humidity [7,8], as well as, substrate wettability [9,10], thermal conductivity and temperature [11,12] on the drop evaporation process. Depending on the surface wettability and surface structure, droplets evaporate in different modes. The widely accepted evaporation mechanisms, depending on the dynamics of the triple contact line (TCL), are the constant contact angle (CCA) mode, the constant contact radius (CCR) mode, and the CCR-CCA mixed mode [13,14]. Typically, the CCA mode happens on smooth hydrophobic substrates where the droplet contact line recedes while the contact angle remains constant to account for the liquid evaporated. On a hydrophilic and/or on a rougher substrate where the surface hysteresis is high though, the triple contact line tends to be pinned while the contact angle decreases with time, namely, the CCR mode. In addition, during evaporation of nanofluid droplets [15,16] or pure fluid droplets on structured surfaces [17], a stick-slip evaporative behavior has also been reported. As a consequence of the different evaporation behavior, the lifetime of a droplet is found to differ [9,18,19]. The evolution, and in particular, the lifetimes, of droplets evaporating in a variety of different modes of evaporation have been studied by Stauber *et el*. [20,21] and Schofield *et al.* [22] using the diffusion-limited evaporation model (see, for example, Popov [18] and Saada *et al*. [23]).

On the other hand, liquid desiccants are a special type of aqueous salt solution, which have excellent hygroscopic properties. Due to the hygroscopic nature of liquid desiccants, they are widely

View Article Online
DOI: 10.1039/C8CP04504F

applied in all kinds of dehumidification systems [24], absorption heat pumps [25,26], and absorption heat transformers [27]. Most commonly used ionic liquid desiccant salts include lithium bromide (LiBr), lithium chloride (LiCl) and calcium chloride ($CaCl_2$) [28]. These salts have strong affinity and adhesion to the water molecules, and after dissolving in water, they reduce greatly the partial vapor pressure of the solution at the liquid-air interface. In the case of droplet evaporation, the vapor diffusion is driven by the vapor pressure difference between the saturated droplet interface and the unsaturated air bulk [29]. Nonetheless, when it comes to liquid desiccant droplets, the vapor pressure at the droplet interface becomes lower than the partial vapor pressure of the ambient air. Therefore, the direction of vapor diffusion converses, and water vapor diffuses spontaneously from the air side to the droplet side.

The coupled heat and mass transfer between humid air and liquid desiccant is fundamental and of significant importance to all kinds of dehumidification applications. Up to now, most of the research carried out on liquid desiccants addresses: the performance of dehumidifiers with different flow patterns [30,31], different type of inner packing [32,33], presence or absence of inner heat sources [34,35], and different desiccant solutions or ambient conditions [36,37], at the macro-scale or at the system scale. Some theoretical models [38] have also been mathematically developed and experimentally verified, which are capable of predicting to some extent the heat and mass transfer process within the dehumidifier as a whole system. Despite of the above mentioned studies, the performance of liquid desiccant droplets within a dehumidifier has been rarely reported. At the inlet of the dehumidifier, desiccant droplets are formed at the liquid distributor before impinging onto the inner packing [39]. Upon impingement, discrete drops varying in size and shape appear at the top of the packing and flow down in a dropwise or filmwise fashion depending on the surface wettability. In

View Article Online
DOI: 10.1039/C8CP04504F

industrial applications, the inner fillers vary from light polymers, non-corrosive ceramics, to high-strength metals [40], which provide different surface wettability, and therefore the flow regime of the desiccant solution inside also differs. A further investigation on vapor absorption into individual liquid desiccant droplets will shed light on the absorption process especially at the initial stage of dehumidification where droplets form and exhibit an initial contact with the substrate. Further understanding on the dynamics of droplet growth during vapor absorption on different substrates will also help providing new insights on the mechanisms of filmwise or dropwise formation and its relation with surface properties, so that one can provide a more accurate prediction of the vapor uptake happening inside different desiccant dehumidification devices.

Hence, in this study, we investigate the vapor absorption mechanisms of LiBr-H_2O droplets on surfaces with different wettability at certain controlled ambient conditions. Experiments are carried out with 54 wt.% aqueous lithium bromide-water (LiBr-H_2O) droplets on hydrophobic polytetrafluoroethylene (PTFE) and on hydrophilic glass substrates commonly used as inner packing in dehumidification systems at laboratory and at industrial scales. The dynamics of triple contact line (TCL) and the evolution of droplet volume are compared, indicating the strong effect of surface wettability on the vapor absorption process into droplets. By looking into the solute diffusion process on the droplet side we demonstrate the different kinetics of absorption and droplet growth function of surface wettability. Moreover, several plausible explanations are provided to account for the apparent droplet spreading phenomenon observed on hydrophilic glass substrates when compared to hydrophobic PTFE one.

View Article Online
DOI: 10.1039/C8CP04504F

2. EXPERIMENTAL SETUP

Experiments are carried out within an insulated environmentally controlled chamber (800L, PR-3KT from ESPEC Corp., Japan), capable of providing constant temperature, T_{amb}, and relative humidity, RH (T_{amb} = -20 ℃ ~ 100 ℃ and RH = 20% ~ 98%) environments. In this study, experiments are carried out at six representative ambient conditions with T_{amb} = 25 ℃ and 45 ℃, and RH = 30%, 60%, and 90%. During experimental observations, the environmental condition within the chamber is monitored both by the chamber panel and by an electronic hygrothermograph (testo 610 from testo AG (Germany), T_{amb} = -10 ℃ ~ 80 ℃ and RH = 20% ~ 100%). Schematic of the experimental setup is shown in Figure 1, which includes: environmental chamber, CCD camera and lens, LED back light, stainless steel laboratory jack, droplet dosing system and data acquisition system. The high-definition CCD camera (Sentech STC-MC152USB with a RICOH lens and 25-mm spacing ring) along with a LED backlight are used to image the droplet profile at 4.8 frames per second. The real-time video of the droplet profile is thereafter processed with the software ImageJ® and MATLAB®. Then, the evolutions of droplet volume, V (μL), contact radius, R (mm), and contact angle, θ (deg), along with time, t (s), are extracted by assuming the shape of the droplet as spherical cap geometry.

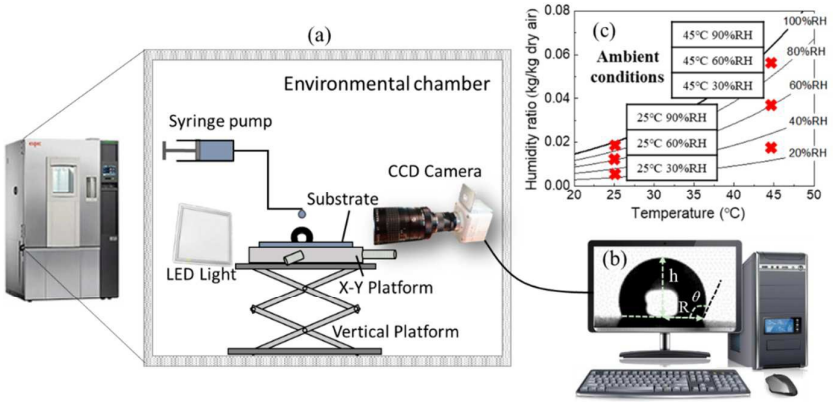

Figure 1 Overview of the experimental setup. (a) Experimental part: environmental chamber, CCD camera, back light, stainless steel vertical platform, X-Y platform, droplet dosing system; (b) data acquisition system with Image J® and Matlab®; (c) Experimental conditions shown on the psychrometric chart.

View Article Online
DOI: 10.1039/C8CP04504F

54.0 wt.% lithium bromide (LiBr) solution and deionized water from Sigma-Aldrich are used as testing fluids for the experimental observations. Typically, a sessile droplet whose largest dimension is smaller than the capillary length will adopt spherical cap shape. For pure water in air, the capillary length is estimated as 2.6 ~ 2.7 mm (calculated according to the definition of capillary length, $\lambda = \sqrt{\gamma_{lg}/\rho g}$ [41], where λ is the capillary length in meters, γ_{lg} is the liquid-air surface tension in N/m, ρ is the liquid density in kg/m^3, g is the gravitational acceleration in m^2/s). On the other hand, for 54 wt.% LiBr- H_2O solution in air, the capillary length is ca. 2.42 mm. In our study, the contact radius of both water droplets and LiBr-H_2O droplets did not exceed the capillary length throughout the vapor absorption process, therefore, the gravity effect on the droplet shape can be neglected and the assumption of treating the droplet as spherical cap is reasonable. We note here that some vapor absorption onto the droplet might happen during droplet deposition.

Table 1 includes the properties of 54.0 wt.% LiBr-H_2O solution and those of pure water. LiBr-H_2O solution has higher viscosity and greater liquid-gas surface tension, which contributes to the higher equilibrium contact angle of LiBr-H_2O droplets on the same substrates when compared to pure water droplets. Moreover, the boiling point of 54 wt.% LiBr-H_2O solution at 1 atmosphere is ca. 40 ℃ higher than that of pure water, which suggests the apparent lower vapor pressure at the solution surface.

Table 1 Properties of 54% wt. LiBr solution and distilled water as specific heat capacity c_p (kJ/kg/K); density ρ (kg/m^3); liquid-gas surface tension γ_{lg} (mN/m); viscosity υ (mPa·s); thermal conductivity k (W/m/K); boiling temperature $T_{boiling}$ (℃). Properties shown were obtained at 20 ℃ and at 1 atm.

Liquid type	c_p (kJ/kg/K)	ρ (kg/m^3)	γ_{lg} (mN/m)	υ (mPa·s)	k (W/m/K)	$T_{boiling}$ (℃)
54% wt. LiBr solution	1.98	1600	91.54	4.751	0.4286	140
Distilled water	4.18	998	72.75	1.005	0.5984	100

View Article Online
DOI: 10.1039/C8CP04504F

Table 2 Properties of glass and PTFE substrates as density ρ (kg/m3); specific heat capacity c_p (J/kg/K); thermal conductivity k (W/m/K); thermal diffusivity α (m^2/s), $\alpha = k/\rho c_p$; surface roughness S_q (μm); and equilibrium contact angle for a 3 μL water droplet, $\theta_{0,W}$ (°), and for a 3 μL LiBr droplet, $\theta_{0,S}$ (°), at 20 ℃ and 1 atm.

Material	ρ (kg/m^3)	c_p (kJ/kg/K)	k (W/m/K)	α (m^2/s)	S_q (μm)	Equilibrium $\theta_{0,W}$ (°)	Equilibrium $\theta_{0,S}$ (°)
PTFE	2200	1.05	0.25	0.52	0.516	98° ± 3°	108° ± 3°
Glass	2400	0.84	0.75	2.15	0.012	70° ± 3°	75° ± 3°

Two types of substrates are chosen for the experiments; hydrophobic polytetrafluoroethylene (PTFE) and hydrophilic glass. Table 2 lists the main properties of the two substrates, where the surface roughness, S_q, is assessed with a 3D optical laser scanning microscope (Olympus LEXT OLS4000, Japan), and the droplet equilibrium contact angle for deionized water, θ_0, is measured using a custom-built contact angle analyzer at laboratory ambient conditions, *i.e.*, T_{amb} = 20 ℃ and 55% *RH*.

Before experiments, substrates are cleaned by immersing each sample in an ultrasonic bath with ethanol for 15 minutes. After that, the sample is taken out and rinsed with large amount of deionized water. Then, substrates are further dried with filtered compressed air to remove any possible remaining dust or contaminants. After drying, the substrate is placed inside the chamber for sufficiently long time for the substrate to reach equilibrium temperature with the environment. Then, a droplet of 4 ± 0.5 μL is deposited within the environmental chamber on the chosen substrate. We note here that dosing system and substrate are inside the chamber for sufficient time to ensure that both fluid and substrate are at T_{amb}. Before droplet deposition, CCD acquisition is started and the evolution of the droplet profile is then recorded in time.

View Article Online
DOI: 10.1039/C8CP04504F

3. EXPERIMENTAL RESULTS

3.1. Droplet TCL dynamics on hydrophilic glass substrates

Representative evolution curves of contact angle, θ, and normalized contact radius, R/R_0, of LiBr-H_2O droplets on a hydrophilic glass substrate for the six different ambient conditions are plotted in Figure 2. The initial contact angle for LiBr-H_2O droplets on a glass substrate is *ca.* 75° ± 3°, about 5° larger than that of pure water droplets due to the higher liquid-air surface tension (see Table 1). Depending on the ambient condition, droplets on hydrophilic glass substrates show different degree of spreading. We note here that the slow spreading evolution reported here differs from early regimes spreading where the droplet establishes the spherical cap in the first few seconds after deposition. Further discussion on the spreading mechanisms is included within Section 4.2. At 30% *RH* (Figure 2(a)), θ decreases from 75° to about 52°, while the contact radius increases to 1.24 times of its initial value. At 60% *RH* (Figure 2(b)) and at 90% *RH* (Figure 2(c)), qualitatively, the decrease in contact angle follows the same trend to that reported for 30% *RH*, where there is an initial decrease and then flattens. Quantitatively, at high humidity of 90% *RH*, the contact angle decreases to about 40° while the contact radius increases to ca. 2 times due to greater drop spreading coupled with greater amount of water vapor absorbed. The quantitative behavior at intermediate humidity of 60% *RH* (Figure 2(b)) is found to lie between low and high relative humidity cases where the contact angle decreases to a value between 40° and 50° and the contact radius increases to a value of ca. 1.4 times the initial one. Ambient temperature T_{amb} is found to influence the rate of droplet spreading during the initial stage of vapor absorption, where the droplet contact angle and contact radius vary more rapidly at 45 ℃ than at 25 ℃.

View Article Online
DOI: 10.1039/C8CP04504F

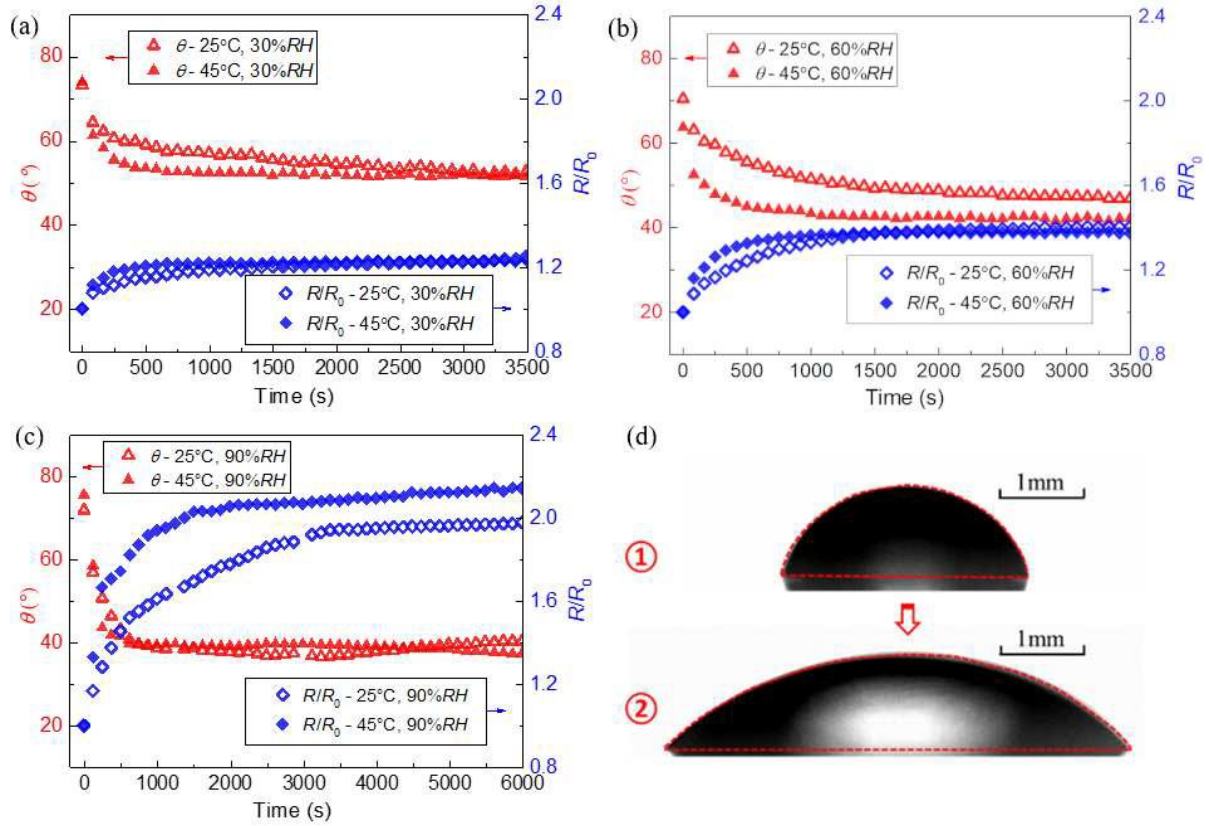

Figure 2 Evolution of (up-triangles) contact angle, θ (°), and (diamonds) normalized contact radius, R/R_0, of LiBr-H_2O droplets, versus time (s) for (a) 30% *RH*, (b) 60% *RH*, and (c) 90% *RH*, at (open symbols) T_{amb} = 25 ℃ and (close symbols) T_{amb} = 45 ℃ on hydrophilic glass substrates. (d) Initial (t = 0 s) and final (t = 6000 s) snapshots of a LiBr-H_2O droplet on a hydrophilic glass substrate at 45 ℃ and 90% *RH*.

To exemplify the droplet profile change during vapor absorption, Figure 2(d) shows snapshots of a LiBr-H_2O droplet on a hydrophilic glass substrate at 45 ℃ and 90% *RH* at the initial (t = 0 s) and at the final (t = 6000 s) stage of absorption. Due to water uptake, an expansion of droplet volume is observed. In addition, due to both droplet expansion and contact angle decrease, the triple contact line (TCL) advances greatly throughout the absorption process, *i.e.*, radius increases to approximately 1.2, 1.4 and 2.0 times its initial value at 30%, 60% and 90% *RH*, respectively.

3.2. Droplet TCL dynamics on hydrophobic PTFE substrates

Representative evolution curves of contact angle, θ, and normalized contact radius, R/R_0, of

View Article Online
DOI: 10.1039/C8CP04504F

LiBr-H_2O droplets on a hydrophobic PTFE substrate for the six different ambient conditions are shown in Figure 3. The initial contact angle of a LiBr-H_2O droplet on the hydrophobic PTFE substrate is *ca.* 108° ± 3° for all the experimental conditions, about 10° higher than that of pure water droplets on the same PTFE substrate studied. At 30% *RH* (Figure 3(a)) the contact angle of a LiBr-H_2O droplet decreases from 108° to 93° ± 4°, while the contact radius increases to ca. 1.2 times its initial value and reaches equilibrium after *ca.* 700 seconds. At 60% *RH* (Figure 3(b)) the droplet contact radius increases to 1.3 times its initial value, while the droplet contact angle decreases from 108° to 93°. At 90% *RH* (Figure 3(c)) the droplet grows even larger as the final R/R_0 reaches *ca.* 1.6, while the contact angle decreases from 107° to 90°. Spreading behavior reported here also differs from early regime spreading where the droplet establishes the spherical cap, which is further discussed within Section 4.2. For the same ambient humidity, the increase in contact radius and the decrease in contact angle are actually more marked at high ambient temperatures (T_{amb} = 45 ℃) than at low ambient temperatures (T_{amb} = 25 ℃).

Moreover, on a PTFE substrate we report the sudden decrease in the contact angle accompanied with the increase in the contact radius in an advancing stick-slip fashion, which is marked with black arrows in Figure 3(b) and Figure 3(c). We henceforth refer to such behavior as advancing stick-slip. For a LiBr-H2O droplet sitting on a hydrophobic PTFE substrate, the TCL remains pinned or slightly increases while the contact angle increases to account for the increase in volume due to vapor absorption (Figure 3(b) and Figure 3(c)). Heterogeneities on the PTFE solid surface may induce the observed additional pinning barrier, which must be overcome before the TCL slips or jumps forward [15, 16]. Typically, as the contact angle deviates from the equilibrium one, the droplet gains certain excess of free energy and when such excess of free energy overcomes the pinning barrier exerted by

View Article Online
DOI: 10.1039/C8CP04504F

the solid surface the jump of the TCL ensues [16]. The advancing slip or jump of the TCL observed is characterized by the sudden decrease in the contact angle and the associated increase in the contact radius. Advancing stick-slip reported here differs from receding stick-slip behavior reported earlier during nanofluid droplet evaporation [15, 16] or pure fluid droplets evaporating on structured surfaces [17]. In the case of receding stick-slip, the contact angle decreases to account for the loss of volume due to evaporation while the TCL remains pinned to the substrate [15, 16]. Then, as the droplet evaporates, the excess of free energy increases and when the excess of free energy becomes greater than the pinning barrier the jump of the TCL ensues [16]. During receding stick-slip the jump of the TCL is characterized by the sudden increase in the contact angle and the associated decrease in contact radius. In addition, the advancing stick-slip appears to be more frequent and marked at high humidity conditions; especially at 90% *RH* (Figure 3(c)), due to the more rapid droplet expansion when compared to 30% *RH* (Figure 3(a)) and to 60% *RH* (Figure 3(b)). To illustrate the vapor absorption behavior, Figure 3(d) shows snapshots of a LiBr-H2O droplet on a hydrophobic PTFE substrate at 45 °C and 90% *RH* at initial droplet deposition (t = 0 s) and at later stage of absorption (t = 6000 s).

View Article Online
DOI: 10.1039/C8CP04504F

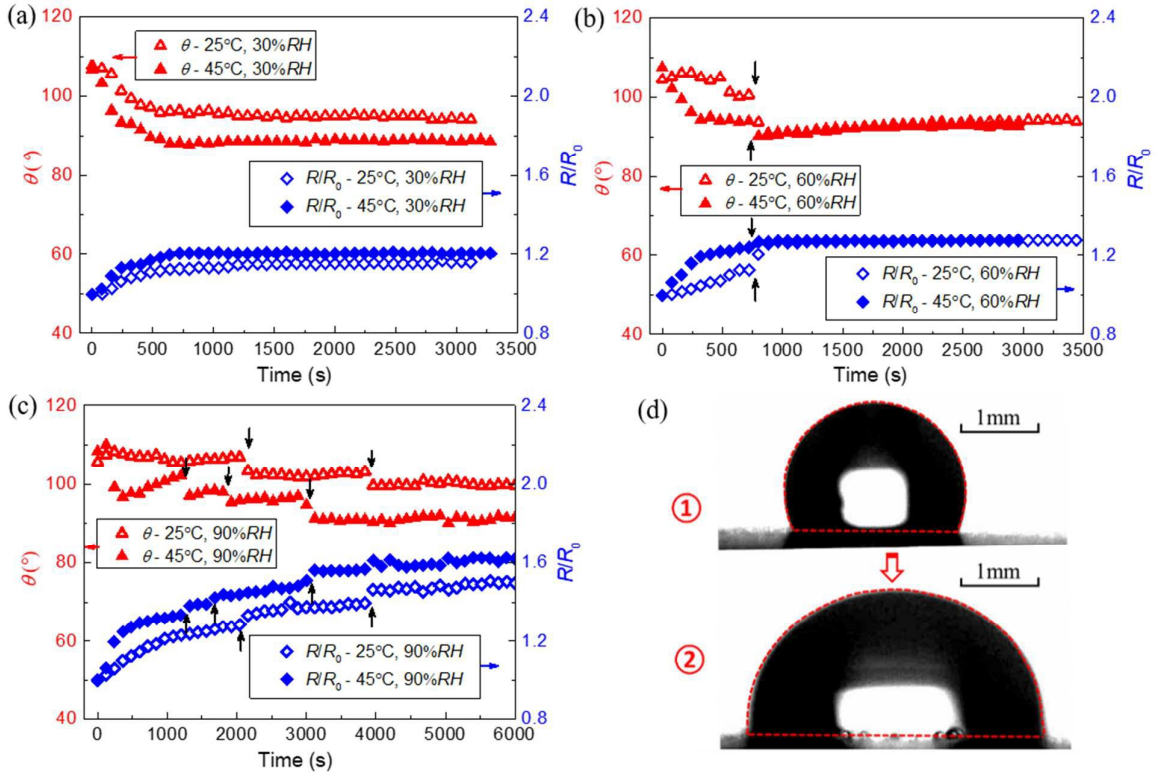

Figure 3 Evolution of (up-triangles) contact angle, θ, and (diamonds) normalized contact radius, R/R_0, of LiBr-H_2O droplets, versus time (s) for (a) 30% *RH*, (b) 60% *RH*, and (c) 90% *RH*, at (open symbols) T_{amb} = 25 ℃ and (close symbols) T_{amb} = 45 ℃ on a hydrophobic PTFE substrate. (d) Initial (t = 0 s) and final (t = 6000 s) snapshots of a LiBr-H_2O droplet on PTFE substrate at 45 ℃ and 90% *RH*.

It is then evident that hygroscopic LiBr-H_2O droplets behave differently depending on the wettability of the surface. The characteristic behavior of absorption for LiBr-H_2O droplets on a hydrophobic PTFE substrate is then characterized by smaller TCL spreading when compared to that observed on hydrophilic glass. On a PTFE substrate the increase of both droplet contact radius and droplet height are solely due to vapor absorption, whereas for LiBr-H_2O droplets on a hydrophilic glass, the coupling mechanisms of both droplet spreading and vapor absorption govern the advancing behavior of the TCL and its dynamics. We also note here that the dynamics of the TCL during vapor absorption into liquid desiccant droplets differ from those of droplet evaporation, droplet condensation, droplet growth upon freezing and/or from the simultaneous monotonic increase in

View Article Online
DOI: 10.1039/C8CP04504F

contact angle and decrease in contact radius due to the water adsorption-absorption and/or condensation during organic solvent evaporation [42-45].

3.3. Evolution of droplet volume during vapor absorption

During vapor absorption, the droplet volume increases in different trends depending on the ambient condition. Figure 4 presents evolution of the normalized droplet volume along with time on hydrophilic glass (Figure 4(a)) and on hydrophobic PTFE substrates (Figure 4(b)). At low ambient humidity of 30% *RH*, the droplet volume increases ca. 10%, and reach equilibrium with the ambient after several hundred seconds. At 60% *RH*, droplets expand more apparently, and it also takes longer for the droplets to reach equilibrium with the ambient, *ca.*1000 ~ 2000 seconds. At high humidity of 90% *RH*, droplets grow following a saturating trend throughout the complete duration of the experimental observations ca. 2 hours. When comparing the final values of the droplet volume in Figure 4, it shows that the final expansion ratio of droplet volume, V_f/V_0, is only related to the relative humidity: V_f/V_0 (30% *RH*) ≈ 1.07, V_f/V_0 (60% *RH*) ≈ 1.5 and V_f/V_0 (90% *RH*) ≈ 2.7 ~ 3.3 regardless of surface wettability and ambient temperature. We note here that although surface wettability does not have an impact on the final droplet volume, there are differences on the absorption kinetics, which will be discussed in the next Section (Section 4).

View Article Online
DOI: 10.1039/C8CP04504F

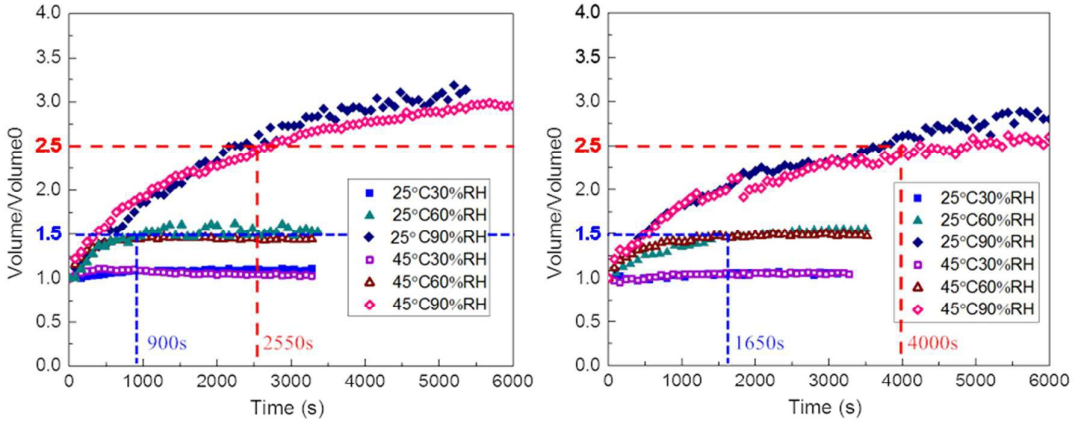

(a) Glass substrate (b) PTFE substrate

Figure 4 Evolution of normalized droplet volume, V/V_0, versus time, t (s), for LiBr-H_2O droplets on (a) glass substrate and (b) PTFE substrate at (close symbols) T_{amb} = 25 ℃ and (open symbols) T_{amb} = 45 ℃ for (squares) 30%, (up-triangles) 60% and (diamonds) 90% *RH*. (Blue dashed line) time at which the droplet reaches V/V_0 = 1.5 at 60% *RH* and (red dashed line) time at which the droplet reaches V/V_0 = 2.5 at 90% *RH*, on a glass and on a PTFE substrate.

As marked with red and blue dashed lines in Figure 4, for the same ambient condition of 45 ℃ and 90% *RH*, on a hydrophobic PTFE substrate it takes 4000 seconds for the LiBr-H_2O droplet to expand to 2.5 times of its initial volume, while on a hydrophilic glass substrate it takes *ca.* 2550 seconds. At 45 ℃ and 60% *RH*, on a hydrophobic PTFE substrate it takes 1650 seconds for the droplets to expand to 1.5 times of its initial volume, while on a hydrophilic glass substrate it takes about half of it, *i.e.*, *ca.* 900 seconds. To provide further quantification and comparison on the amount of water uptake during the absorption process, Table 3 presents the normalized droplet volume at different instants of time with t = 0 s as the droplet deposition. On one hand, at low relative humidity 30% *RH* the droplet volume remains constant during the absorption times reported in Table 3. On the other hand, when looking into medium and high relative humidity conditions, i.e., 60% *RH* and 90% *RH*, the droplet volume increases faster on hydrophilic glass when compared to hydrophobic PTFE. We note here that in the case of high relative humidity 90% *RH*, the droplet volume continuously increases for the experimental times reported.

View Article Online
DOI: 10.1039/C8CP04504F

Table 3 Normalized droplet volume, V/V_0, at 25 °C and 30%, 60% and 90% *RH* on both hydrophilic glass and hydrophobic PTFE substrates at t = 500, 1000, 2000, 3000 and 4000 seconds with t = 0 seconds as the droplet deposition instant.

Normalized droplet volume, V/V_0, at 25 ℃	500 s		1000 s		2000 s		3000 s		4000 s	
	glass	PTFE	glass	PTFE	glass	PTFE	glass	PTFE	glass	PTFE
30% *RH*	1.06	1.09	1.09	1.09	1.10	1.11	1.11	1.11	-	-
60% *RH*	1.32	1.33	1.55	1.48	1.60	1.57	1.61	1.63	-	-
90% *RH*	1.49	1.46	1.82	1.75	2.33	2.16	2.73	2.39	2.89	2.52

To demonstrate the amount of water absorbed during droplet expansion depending on T_{amb} and *RH*, Figure 5 includes the psychometric chart representing the humidity ratio (kg water/ kg dry air) versus T_{amb} and *RH*. The properties of LiBr-H_2O solution and humid air in the chart are calculated with embedded functions in EES® (Engineering Equation Solver) software. Black solid lines in Figure 5 show the condition (T_{amb} and humidity ratio) of ambient air at different *RH*, while blue dashed lines represent the condition (T_{amb} and humidity ratio) of the equivalent humid air layer at the surface of LiBr-H_2O solution with different concentrations. It can be seen that the iso-concentration curves of LiBr-H_2O solution and the iso-relative humidity curves of ambient air are in parallel or overlap with each other, which indicates that the humid air at a certain relative humidity is in equilibrium with the solution for a certain salt concentration. When the ambient relative humidity keeps constant, the desiccant droplet will keep absorbing water vapor until it reaches equilibrium with the ambient.

View Article Online
DOI: 10.1039/C8CP04504F

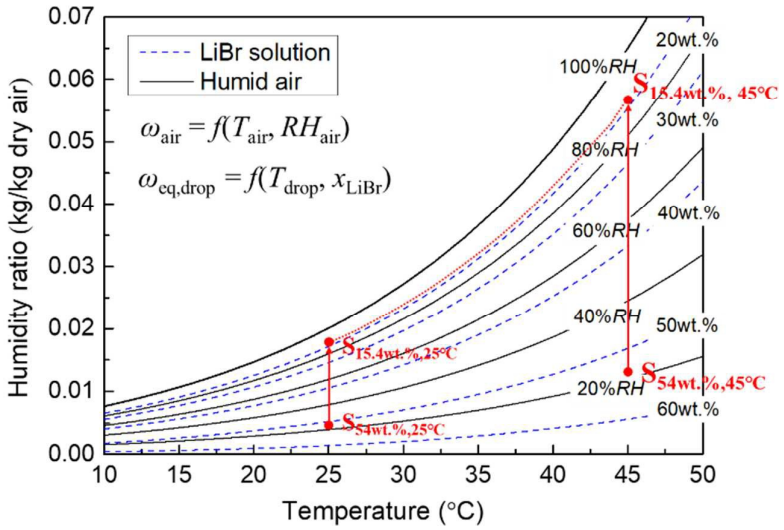

Figure 5 Psychrometric chart showing the condition of the humid air (solid line) at different relative humidity, and the condition of equivalent humid air layer at the surface of LiBr-H_2O solution (blue dashed line) at different concentrations. Red solid arrows present the concentration variation of LiBr-H_2O solution during vapor absorption.

The red points in Figure 5 represent the initial and final conditions($S_{initial,25℃}$, $S_{final,25℃}$, $S_{initial,45℃}$, $S_{final,45℃}$) of the LiBr-H_2O droplets at 25 ℃, 45 ℃, and 90% *RH*. During vapor absorption, the liquid desiccant salts stay within the droplet in the form of ions, and therefore, the solution concentration of LiBr, x, should follow the solute conservation equation shown in Eq. (1):

$$\rho_{initial} V_{initial} x_{initial} = \rho_{final} V_{final} x_{final} \tag{1}$$

For droplets at 25 ℃ and 45 ℃, the expansion ratio of droplet volume is therefore derived as:

$$\left(\frac{V_{final}}{V_{initial}}\right)_{25°C} = \left(\frac{x_{initial}}{x_{final}}\right)_{25°C} \left(\frac{\rho_{initial}}{\rho_{final}}\right)_{25°C}, \quad \left(\frac{V_{final}}{V_{initial}}\right)_{45°C} = \left(\frac{x_{initial}}{x_{final}}\right)_{45°C} \left(\frac{\rho_{initial}}{\rho_{final}}\right)_{45°C} \tag{2}$$

Taking 90% *RH* as an example, the $\rho_{initial}/\rho_{final}$ is 1.430 at 25 ℃, and 1.433 at 45 ℃ according to our calculation based on the correlation provided in Ref. [46]. And since the ratio of droplet concentration $x_{initial}/x_{final}$ is also the same for 25 ℃ and for 45 ℃, the same final expansion ratio of droplet volume $V_{final}/V_{initial}$ regardless of the ambient temperature and surface wettability is then demonstrated.

View Article Online
DOI: 10.1039/C8CP04504F

4. ANALYSIS AND DISCUSSION

4.1. Effect of surface wettability on the absorption kinetics

From the evolution of droplet volume, it is also worth noticing that the surface wettability has a strong effect on the kinetics of vapor absorption and on the dynamics of the TCL, which in turn dictates the mechanisms of droplet growth. Further quantification of the results presented in Section 3 is included in Table 4, which shows the normalized vapor absorption rates for the first 100 seconds after the droplet deposition. Droplets on hydrophilic glass substrates show higher vapor absorption rates than those on hydrophobic PTFE. In addition, the expected greater initial absorption rates at high ambient temperature (T_{amb} = 45 °C) when compared to low ambient temperature (T_{amb} = 25 °C) are also highlighted.

Table 3 Normalized initial vapor absorption rate, $d(V/V_0)/dt$, during the first 100 seconds for: 25℃ - 60% *RH*, 25℃ - 90% *RH*, 45℃ - 60% *RH*, and 45℃ - 90% *RH*, on hydrophilic glass and hydrophobic PTFE substrates.

Normalized absorption rate $d(V/V_0)/dt$ (s^{-1})	25℃ - 60%*RH*	25℃ - 90%*RH*	45℃ - 60%*RH*	45℃ - 90%*RH*
Hydrophilic glass	0.00102	0.00103	0.00137	0.00132
Hydrophobic PTFE	0.00098	0.00089	0.00133	0.00124

Droplet growth due to vapor uptake into liquid desiccant droplets reported in this study is driven by the vapor pressure difference between the humid air and the droplet surface. The vapor absorption from the humid air into the LiBr-H_2O droplet can be divided into three steps: the water vapor diffusion on the air side, the vapor to water phase-change transition at the air-liquid interface, and the diffusion of water molecules from the droplet interface toward the droplet bulk (or the solute (Li^+, Br^-) diffusion from the bulk of the droplet towards the droplet interface). Figure 6 shows one-dimensional evolution of ambient air and liquid desiccant solution during the vapor absorption

View Article Online
DOI: 10.1039/C8CP04504F

process, where the thickness of the liquid layer for the diffusion of the solute equals the droplet characteristic length (h^*), and the air layer is assumed to be infinite since the chamber is large enough compared to the size of the droplets. At the very initial stage, right after the droplet deposition (t = 0 seconds), we assume that there is no mass diffusion between the humid air and the aqueous solution, and an apparent vapor pressure difference between the ambient air and the liquid surface is present. Then, driven by the pressure difference, water vapor gradually diffuses from the air side to the liquid-air interface, and gets absorbed. Due to vapor absorption, the concentration of solute (Li^+ and Br^- ions) near the liquid-air interface decreases. Then, Li^+ and Br^- ions diffuse from the high concentration side at the droplet bulk to the low concentration side at the liquid interface following the concentration gradient. As the absorption process continues and as a consequence of the increase in water concentration within the droplet, the vapor pressure difference between the liquid surface and the ambient air decreases. At the same time, the concentration gradient of LiBr solute within the aqueous solution also decreases until equilibrium is attained. The local change in concentration at the liquid-air interface and in the droplet profile due to vapor absorption reported here, differs from the concentration change due to preferential evaporation of one component during evaporation of binary mixtures [43, 47-49].

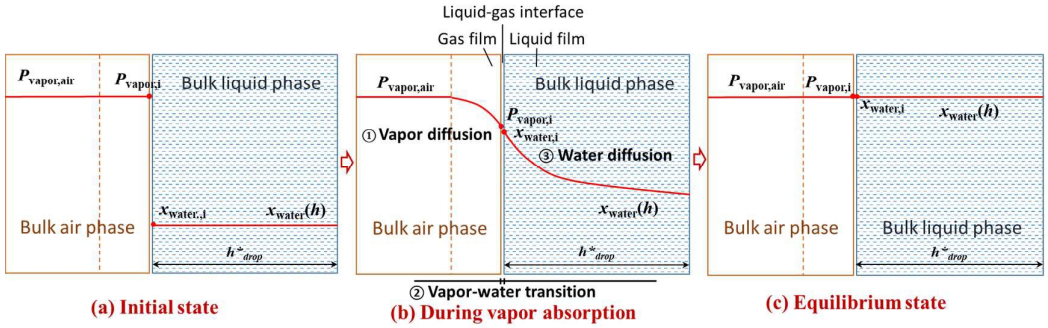

Figure 6 Schematic of water vapor concentration in the air side and the concentration of liquid water in the bulk of the droplet (a) at initial stage right after droplet deposition, t = 0 s, (b) during vapor absorption, and (c) at equilibrium, $t = \infty$.

View Article Online
DOI: 10.1039/C8CP04504F

Since vapor absorption is a surface area related problem, it is noteworthy providing a comparison between the spherical cap surface area of liquid desiccant droplets on hydrophilic *versus* hydrophobic_substrates. For droplets on hydrophilic glass substrate, the interfacial area for mass transfer is *ca.* 9.02~10.65 mm^2, while for droplets on hydrophobic PTFE, the interfacial area is *ca.* 9.04~10.68 mm^2. Since there is no large difference in the effective droplet areas for vapor absorption, the absorption rate must be governed by the mass diffusion process on the air side and/or on the liquid side. Typically, the mass diffusion rate in the liquid phase is $10^3 \sim 10^4$ times of that in the gas phase ($D_{\mathrm{water/air}}/D_{\mathrm{LiBr/LiBr-H_2O}} \sim 10^{-5}/10^{-9} \sim 10^4$) [50]. Therefore, we can assume that the vapor absorption process is limited by the solute diffusion on the liquid side.

The solute diffusion process within the LiBr-H_2O droplet can be further evaluated by the characteristic time, τ, presented as Eq. (3),

$$\tau = L^2/D \tag{3}$$

where L is the characteristic length for mass diffusion, which we assume as the characteristic length of the droplet, h^*, and D is the mass diffusion rate (m^2/s).

According to eq. (3), the characteristic time for the solute diffusion on the liquid side is calculated as ca. 10^3 seconds, where the characteristic length of the droplet, L, is estimated as 1 mm, and the water diffusion rate, D_s, is 10^{-9} m^2/s [51, 52]. It shows that the characteristic time for solute diffusion is in the same order of magnitude to that of the vapor absorption period reported in the experiments (500 ~ 8000 seconds). Hence, solute concentration gradient within the LiBr-H_2O droplet is the dominant mechanism governing vapor absorption onto liquid desiccant droplets and cannot be neglected.

Considering the solute diffusion process within the droplet governed by Fick's law, the

View Article Online
DOI: 10.1039/C8CP04504F

368 characteristic length for solute diffusion is the shortest path for the diffusing molecules of water to
369 reach the solid surface and for the Li^+ and Br^- molecules to reach the liquid-air interface, or to "meet"
370 each other. While the solid surface can be treated as an impermeable boundary with zero mass flux,
371 the liquid-air interface must be treated as a moving boundary condition governed by the change in
372 droplet volume due to water vapor absorption. On hydrophilic glass substrates where the droplet
373 contact angle is less than 90°, the characteristic length for solute diffusion required for the theoretical
374 description of this process is the droplet height $h^* = h_{drop}$ as shown in Figure 7(a). Whereas on
375 hydrophobic PTFE substrates where the droplet contact angle is larger than 90°, the characteristic
376 length for solute diffusion is the radius of curvature $h^* = \kappa_{drop}$ as shown in Figure 7(b). Further work
377 is currently being sought on the theoretical modelling of the vapor absorption process.

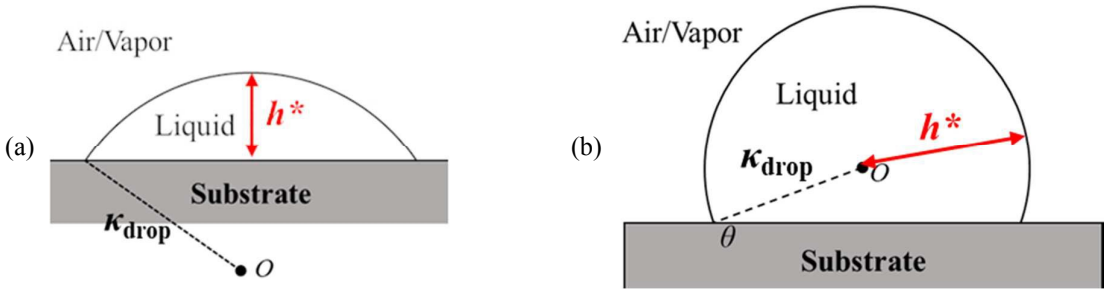

378 Figure 7 Characteristic droplet length, h^*, for solute diffusion within the LiBr-H_2O droplets (a) on hydrophilic
379 glass substrate, and (b) on hydrophobic PTFE substrates.

380 Figure 8 shows the evolution of the characteristic lengths for droplets on a hydrophilic glass
381 substrate and on a hydrophobic PTFE substrate in time at 45 ℃ and 60% *RH* (Figure 8(a)) and at 45 ℃
382 and 90% *RH* (Figure 8(b)). It shows that on glass substrates the characteristic length (droplet height)
383 decreases along with time at 60% *RH* as a consequence of the reported droplet spreading. While at
384 90% *RH* the characteristic length actually increases due to the greater amount of absorbed water
385 vapor when compared to 60% *RH*. By comparison, on PTFE substrates the characteristic length

View Article Online
DOI: 10.1039/C8CP04504F

(radius of curvature) increases to greater extent when compared to the characteristic length reported on hydrophilic glass substrates (Figure 8). At 60% *RH* the characteristic length increases from about 1.18 mm to about 1.4 mm in 3500 seconds, while at 90% *RH*, the characteristic length increases from about 1.1 mm to about 1.7 mm in 7000 seconds.

The characteristic time τ for mass diffusion defined in Equation 3, accounts for how long it takes for the water molecules to diffuse over the distance h^*, hence as h^* increases so does τ, and droplet saturation is reached later on the hydrophobic case. At 45 ℃ and 60% *RH*, for the same diffusion coefficient, $\tau_{\mathrm{PTFE}}/\tau_{\mathrm{glass}} \sim h^*_{PTFE}/h^*_{glass} \sim$ 1.96. This estimation remarkably agrees with the experimental results where it takes 1650 seconds and 900 seconds for the droplets to reach equilibrium on PTFE substrate and on glass substrate respectively, *i.e.*, τ_{PTFE} / τ_{glass} = 1650 / 900 ~ 1.83.

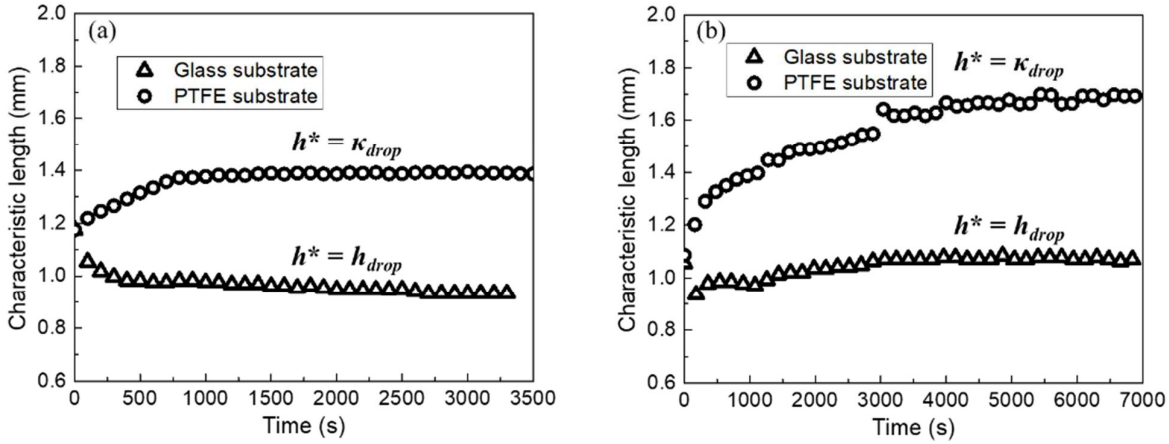

Figure 8 Evolution of characteristic lengths for solute diffusion within the LiBr-H_2O droplets, versus time (s), on (triangles) hydrophilic glass substrates and on (circles) hydrophobic PTFE at (a) 45 ℃ and 60% *RH*, and at (b) 45 ℃ and 90% *RH*.

The above analysis clearly demonstrates that surface wettability has a strong impact on the mechanisms of growth and spreading of hygroscopic lithium bromide desiccant droplets. Due to the shorter characteristic length for solute diffusion, droplets on hydrophilic glass substrate show faster

View Article Online
DOI: 10.1039/C8CP04504F

vapor absorption rates. Since the efficiency and dehumidification capacity of packed towers are closely related to the vapor absorption rate of the liquid desiccant, for industrial applications, we then propose hydrophilic inner packing as the optimum configuration to further enhance the efficiency and dehumidification capacity of such systems. .

4.2. Mechanisms of droplet spreading during vapor absorption

As described in Section 3, on hydrophilic glass substrates LiBr-H_2O droplets show a clear spreading trend with monotonically increasing contact radius and decreasing contact angle (Figure 2), while on hydrophobic PTFE substrates no apparent additional spreading is observed (Figure 3). We note here that right after droplet deposition, there is a competition between capillary and viscous dissipation forces occurring within the first instant after deposition prompting the spherical cap shape of the droplet. This initial transient spreading differs from the timescales of spreading reported on hydrophilic glass substrates upon vapor absorption. In previous literature, droplet spreading phenomenon is reported in the droplet deposition process [53]. In those studies, the droplet spreading is due to competition between capillary driving forces and viscous dissipation, and takes place within the first seconds right after droplet deposition following Tanner's law [54]: $R(t) \propto t^{1/10}$. The time scale of spreading is in the order of milliseconds for low viscosity liquids such as water in air on boro-silicate glass substrates [53] or hexadecane on copper and/or glass [55]. However, in our work LiBr-H_2O droplets spread along with a time scale ca. 10^2~10^3 s greater than for early regimes of spreading. Therefore, classical droplet spreading described by Tanner's law cannot be used to explain the spreading of the TCL observed during vapor absorption on a hydrophilic substrate.

Next, to elucidate the different spreading behavior depending on the substrate wettability

View Article Online
DOI: 10.1039/C8CP04504F

reported in our study, we look into the different binary interactions at the TCL. Seemingly, to the phenomena taking place during receding stick-slip earlier reported in literature, during vapor absorption on a hydrophobic PTFE surface the TCL remains pinned to the surface because of the intrinsic energy barrier presumably induced by substrate heterogeneities [16,56,57]. Then, the contact angle increases to account for the increase in droplet volume. As the contact angle deviates from that of equilibrium, the droplet gains certain excess of free energy [57,58]. As the excess of free energy overcomes the intrinsic energy barrier induced by the solid substrate the jump or slip of the contact line takes place [15, 16, 57, 58]. Next, we provide a qualitative local force balance at the TCL for establishing the different nature of the intrinsic energy barrier depending on the wettability of the surface, similar to the one proposed by Shanahan [16, 57, 58]. Figure 9 presents schematic of the droplet profile at equilibrium contact angle, θ_0, and at slightly larger contact angle when respect to the equilibrium one, $\theta_0+\delta\theta$, due to vapor absorption on (a) hydrophilic glass and (b) on hydrophobic PTFE substrates. At the equilibrium state, the profile of a droplet on a smooth ideal surface follows the balanced Young's equation, $\gamma_{SG} - \gamma_{SL} = \gamma_{LG}\cos\theta_0$, which accounts for the respective binary surface tensions: solid-gas, γ_{SG}, solid-liquid, γ_{SL}, and liquid-gas, γ_{LG} [59]. As conveyed above, after the deposition of a desiccant droplet on a substrate in the presence of a humid environment, the droplet volume will increase due to vapor absorption. Within a finite short time, δt, and assuming the droplet contact line as pinned, the contact angle will increase due to volume expansion to ($\theta_0+\delta\theta$). Moreover, since the solution near the droplet surface gets diluted due to water absorption, the liquid-gas surface tension γ_{LG} will decrease by $\delta\gamma_{LG}$. Due to the variations in both the contact angle and the liquid-gas surface tension, the force balance at the TCL is altered, and as a consequence an extra horizontal force, δF, arises which tends to depin the contact line. By neglecting the second order small quantity,

View Article Online
DOI: 10.1039/C8CP04504F

δF can be derived as Eq. (4):

$$\delta F = \left(\gamma_{LG} - \delta\gamma_{LG}\right)\cos\left(\theta_0 + \delta\theta\right) - \gamma_{LG}\cos\theta_0 \approx -\gamma_{LG}\sin\theta_0\delta\theta - \delta\gamma_{LG}\cos\theta_0 \quad (4)$$

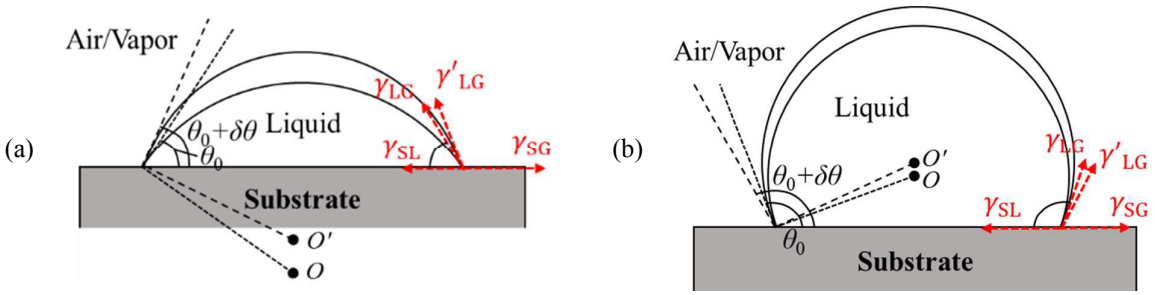

Figure 9 Schematic of droplet profiles at the equilibrium state and at a slightly different contact angle when compared to equilibrium one ($\theta_0 \rightarrow \theta_0+\delta\theta$) due to vapor absorption on (a) hydrophilic glass substrate and on (b) hydrophobic PTFE substrate.

On hydrophilic substrates, the droplet contact angle is smaller than 90°, and the value of $\cos\theta_0$ is positive. In this case, the absolute value of the depinning force can be expressed as $\left|\delta F\right|_{\theta<90^\circ} = \left|\gamma_{LG}\sin\theta_0\delta\theta\right| + \left|\delta\gamma_{LG}\cos\theta_0\right|$. While on hydrophobic substrates, the contact angle is larger than 90°, and the absolute value of the depinning force can be then expressed as $\left|\delta F\right|_{\theta>90^\circ} = \left|\gamma_{LG}\sin\theta_0\delta\theta\right| - \left|\delta\gamma_{LG}\cos\theta_0\right|$. Therefore, for the same change in the contact angle, the depinning force is larger on hydrophilic substrates than on hydrophobic ones: $\left|\delta F\right|_{\theta<90^\circ} > \left|\delta F\right|_{\theta>90^\circ}$. Then, for an identical intrinsic energy barrier, $\partial U/\partial r$, it is easier for the TCL to advance on hydrophilic glass substrates.

Figure 10 shows the evolution of liquid-air surface tension, γ_{LG}, along with vapor absorption for the six experimental conditions studied by assuming the solute distribution within the droplet as homogenous [60]. Depending on the experimental condition investigated, γ_{LG} of LiBr-H_2O droplet decreases as water vapor is absorbed. In addition, as for common fluids, at higher temperature, LiBr-H_2O droplets have smaller surface tension than at low temperatures. Moreover, as absorption takes place, the surface tension decreases with time and changes in surface tension are more marked

View Article Online
DOI: 10.1039/C8CP04504F

at higher ambient humidity conditions as shown in Figure 10. In the extreme case of 45 ℃ and 90% RH, the surface tension decreases from ca. 88.04 mN/m to ca. 74.78 mN/m, which is still larger than that of pure water droplet at 45 ℃ ($\gamma_{LG,water,45℃} \approx$ 69.14mN/m [61]). The decrease in the droplet surface tension partly accounts for the contact angle decrease during vapor absorption. Nevertheless, the decrease in contact angle during vapor absorption is about 30°, which cannot be accounted for by the contact angle change caused purely by the decrease in surface tension. Therefore, additional explanations are expected.

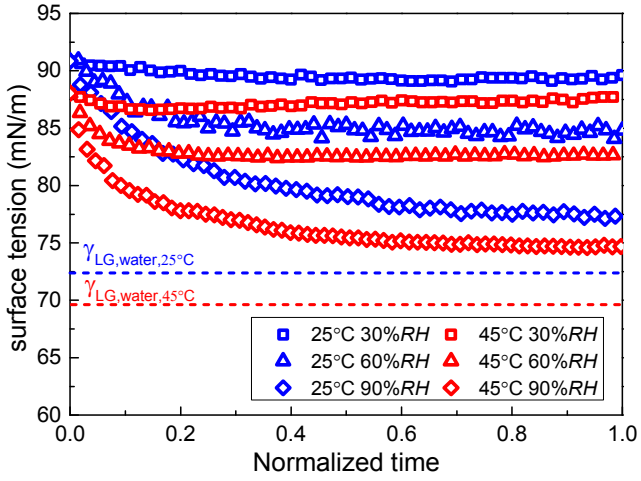

Figure 10 Evolution of surface tension of LiBr-H_2O droplets along with time during vapor absorption on a hydrophilic glass substrate.

Compared to hydrophobic PTFE substrates, the hydrophilic nature of glass substrates induces higher adhesion force to water molecules [62]. Therefore, in humid environments, water molecules may accumulate near the glass surface due to adsorption [63]. In the presence of a LiBr-H_2O droplet, the surface near the contact line will absorb more water vapor and induce both density gradient and surface tension gradient along the droplet interface. In previous literature, droplet spreading has been observed under surface tension gradients induced by localized surfactant addition [64], as well as by an imposed temperature gradient [65]. Therefore, the density gradient and surface tension gradient

View Article Online
DOI: 10.1039/C8CP04504F

induced by non-uniform absorption across the droplet surface can be another plausible reason for the droplet spreading observed in this study.

Furthermore, when looking into a moving contact line, a precursor film is usually considered to be ahead of the visible droplet bulk [66-68]. In previous studies, the existence of precursor film has been verified by advanced experimental techniques such as atomic force microscopy (AFM) [69], and epifluorescence inverted microscopy [70], amongst others [71]. Figure 11 shows the proposed schematic of the continuous transition from the macroscopic droplet profile to the microscopic precursor film at the triple contact line for a spreading droplet on a hydrophilic substrate. The length of the diffusive precursor film is proportional to the square root of time and can be expressed as Eq. (5) [70].

$$L_p = \sqrt{\frac{A}{3\pi\eta h_c}} t^{1/2} \tag{5}$$

where L_p is the length of the precursor film, A is the effective Hamaker constant, η is viscosity, h_c is the cutoff thickness, and t is time.

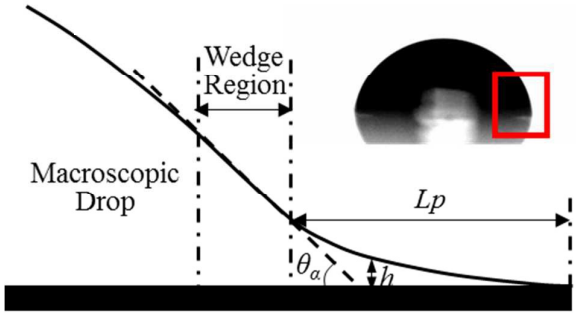

Figure 11 Schematic of microscopic features in the vicinity of the advancing contact line on a hydrophilic substrate as: precursor film ahead of the visible macroscopic droplet [70], wedge region and macroscopic droplet. Macroscopic droplet profile is also included along.

For droplets on a hydrophobic PTFE substrate, due to the larger droplet curvature, the cutoff

View Article Online
DOI: 10.1039/C8CP04504F

thickness is larger than that of droplets on hydrophilic glass [72]. According to Eq. (5), the length of the precursor film is inversely proportional to the square root of the cutoff thickness, hence the length of precursor film will be. During experiments, vapor absorption happens both at the macroscopic droplet interface and at the precursor film. As vapor absorption proceeds, the precursor film will gradually grow thicker, with the inner side merging with the droplet bulk, and the outer side stretching forward. Since the precursor film typically extends more on hydrophilic substrates than that on hydrophobic ones, the precursor film develops more rapidly, and the triple contact line thus advances further, which is put forward as an additional mechanism for the greater droplet spreading observed on hydrophilic substrates.

5. CONCLUSIONS

The present study provides novel fundamental insights in vapor absorption process into single liquid hygroscopic desiccant droplets providing a new sub-topic of research on droplets. The effect of substrate wettability and ambient conditions are explored. Typically, on hydrophilic glass substrates, LiBr-H_2O droplets show a spreading trend during vapor absorption. While on hydrophobic PTFE substrates, the smaller decrease in the contact angle along with an increasing contact radius evidences the lower spreading behavior when compared to hydrophilic glass. Moreover, the final volume expansion ratio of droplet is only function of relative humidity regardless of ambient temperature and surface wettability.

Depending on the wettability of the substrate, the kinetics of vapor absorption are found to differ. On hydrophilic glass substrates, LiBr-H_2O droplets reach equilibrium with the ambient much quicker when compared to hydrophobic PTFE substrates. This is attributed to the shorter characteristic length

View Article Online
DOI: 10.1039/C8CP04504F

for solute diffusion, which is further demonstrated by evaluating the characteristic time for solute diffusion within the droplet.

Besides, the apparent droplet spreading on hydrophilic glass substrates is explained based on a force balance analysis at the triple contact line, by the evolution of liquid-gas droplet surface tension, and by the development of a precursor film during vapor absorption.

To summarize, the vapor uptake into single liquid desiccant droplets and the mechanisms of droplet growth and spreading are revealed. The presented findings are of great significance both for a more accurate prediction of the vapor absorption process and for the optimization of dehumidification devices.

Conflict of Interests

The authors declare that they have no conflict of interests.

Acknowledgements

The authors gratefully acknowledge the support received by the International Institute for Carbon-Neutral Energy Research (WPI-I^{2}CNER) and the Inter Transdisciplinary Energy Research Support Program from Kyushu University. ZW acknowledges the support received by the Japanese Society for the Promotion of Science (JSPS). DO gratefully acknowledges the support received from JSPS KAKENHI (Grant no. JP16K18029 and JP18K13703).

References

[1] Park, J., & Moon, J. "Control of colloidal particle deposit patterns within picoliter droplets ejected by ink-jet printing." *Langmuir* 22.8 (2006): 3506-3513.

View Article Online
DOI: 10.1039/C8CP04504F

[2] Brinker, C. J., Lu, Y., Sellinger, A., & Fan, H. "Evaporation-induced self-assembly: nanostructures made easy." *Advanced Materials* 11.7 (1999): 579-585.

[3] Ming, T., Kou, X., Chen, H., Wang, T., Tam, H. L., Cheah, K. W., Chen J. Y & Wang, J. "Ordered gold nanostructure assemblies formed by droplet evaporation." *Angewandte Chemie* 120.50 (2008): 9831-9836.

[4] Dugas, V., Broutin, J., & Souteyrand, E. "Droplet evaporation study applied to DNA chip manufacturing." *Langmuir* 21.20 (2005): 9130-9136.

[5] Sefiane, K., Wilson, S. K., David, S., Dunn, G. J., & Duffy, B. R. "On the effect of the atmosphere on the evaporation of sessile droplets of water." *Physics of Fluids* 21.6 (2009): 062101.

[6] Sefiane, K. "Effect of nonionic surfactant on wetting behavior of an evaporating drop under a reduced pressure environment." *Journal of Colloid and Interface Science* 272.2 (2004): 411-419.

[7] Girard, F., Antoni, M., Faure, S., & Steinchen, A. "Influence of heating temperature and relative humidity in the evaporation of pinned droplets." *Colloids and Surfaces A: Physicochemical and Engineering Aspects* 323.1 (2008): 36-49.

[8] Fukatani, Y., Orejon, D., Kita, Y., Takata, Y., Kim, J., & Sefiane, K. "Effect of ambient temperature and relative humidity on interfacial temperature during early stages of drop evaporation." *Physical Review E* 93.4 (2016): 043103.

[9] McHale, G., Aqil, S., Shirtcliffe, N. J., Newton, M. I., & Erbil, H. Y. "Analysis of droplet evaporation on a superhydrophobic surface." *Langmuir* 21.24 (2005): 11053-11060.

[10] Patil, N. D., Bange, P. G., Bhardwaj, R., & Sharma, A. "Effects of substrate heating and wettability on evaporation dynamics and deposition patterns for a sessile water droplet containing colloidal particles." *Langmuir* 32.45 (2016): 11958-11972.

[11] Dunn, G. J., Wilson, S. K., Duffy, B. R., David, S., & Sefiane, K. "The strong influence of substrate conductivity on droplet evaporation." *Journal of Fluid Mechanics* 623 (2009): 329-351.

[12] Zhong, X., & Duan, F. "Disk to dual ring deposition transformation in evaporating nanofluid droplets from substrate cooling to heating." *Physical Chemistry Chemical Physics* 18.30 (2016): 20664-20671.

[13] Bansal, L., Chakraborty, S., & Basu, S. "Confinement-induced alterations in the evaporation dynamics of sessile droplets." *Soft Matter* 13.5 (2017): 969-977.

[14] Xu, W., Leeladhar, R., Kang, Y. T., & Choi, C. H. "Evaporation kinetics of sessile water droplets on micropillared superhydrophobic surfaces." *Langmuir* 29.20 (2013): 6032-6041.

[15] Askounis, A., Orejon, D., Koutsos, V., Sefiane, K., & Shanahan, M. E. "Nanoparticle deposits near the contact line of pinned volatile droplets: size and shape revealed by atomic force microscopy." *Soft Matter* 7.9 (2011): 4152-4155.

[16] Orejon, D., Sefiane, K., & Shanahan, M. E. "Stick–slip of evaporating droplets: substrate hydrophobicity and nanoparticle concentration." *Langmuir* 27.21 (2011): 12834-12843.

View Article Online
DOI: 10.1039/C8CP04504F

[17] Antonini, C., Lee, J. B., Maitra, T., Irvine, S., Derome, D., Tiwari, M. K., Carmeliet, J., Poulikakos, D. "Unraveling wetting transition through surface textures with X-rays: Liquid meniscus penetration phenomena." *Scientific Reports* 4 (2014): 4055.

[18] Popov, Y. O. "Evaporative deposition patterns: Spatial dimensions of the deposit." *Physical Review E* 71 (2005): 036313.

[19] Shanahan, M. E. R., Sefiane, K., & Moffat, J. R., "Dependence of Volatile Droplet Lifetime on the Hydrophobicity of the Substrate." *Langmuir* 27.8 (2011): 4572-4577.

[20] Stauber, J. M., Wilson, S. K., Duffy, B. R., & Sefiane, K. "On the lifetimes of evaporating droplets." *Journal of Fluid Mechanics* 744 (2014): R2.

[21] Stauber, J. M., Wilson, S. K., Duffy, B. R., Sefiane, K., "On the lifetimes of evaporating droplets with related initial and receding contact angles." *Physics of Fluids* 27 (2015): 122101.

[22] Schofield, F. G. H., Wilson, S. K., Pritchard, D., Sefiane, K., "The lifetimes of evaporating sessile droplets are significantly extended by strong thermal effects." *Journal of Fluid Mechanics* 851 (2018): 231—244.

[23] Saada, M. A., Chikh, S., & Tadrist, L., "Evaporation of a sessile drop with pinned or receding contact line on a substrate with different thermophysical properties" *International Journal of Heat and Mass Transfer* 58 (2013):197-208.

[24] Mei, L., & Dai, Y. J. "A technical review on use of liquid-desiccant dehumidification for air-conditioning application." *Renewable & Sustainable Energy Reviews* 12.3 (2008):662-689.

[25] Chua, K. J., Chou, S. K., & Yang, W. M. "Advances in heat pump systems: A review." *Applied Energy* 87.12 (2010): 3611-3624.

[26] Wang, Z., Zhang, X., & Li, Z. "Evaluation of a flue gas driven open absorption system for heat and water recovery from fossil fuel boilers." *Energy Conversion and Management* 128 (2016): 57-65.

[27] Parham, K., Khamooshi, M., Tematio, D. B. K., Yari, M., & Atikol, U. "Absorption heat transformers–a comprehensive review." *Renewable and Sustainable Energy Reviews* 34 (2014): 430-452.

[28] Chua, K. J., Chou, S. K., & Yang, W. M. "Liquid desiccant materials and dehumidifiers – A review." *Renewable & Sustainable Energy Reviews* 56 (2016):179-195.

[29] Hu, H., & Larson, "Evaporation of a sessile droplet on a substrate." *The Journal of Physical Chemistry B* 106.6 (2002): 1334-1344.

[30] Liu, X. H., Zhang, Y., Qu, K. Y., & Jiang, Y. "Experimental study on mass transfer performances of cross flow dehumidifier using liquid desiccant." *Energy Conversion and Management* 47.15 (2006): 2682-2692.

[31] Longo, G. A., & Gasparella, A. "Experimental and theoretical analysis of heat and mass transfer in a packed column dehumidifier/regenerator with liquid desiccant." *International Journal of Heat and Mass Transfer* 48.25 (2005): 5240-5254.

View Article Online
DOI: 10.1039/C8CP04504F

[32] Dai, Y. J., & Zhang, H. F. "Numerical simulation and theoretical analysis of heat and mass transfer in a cross flow liquid desiccant air dehumidifier packed with honeycomb paper." *Energy Conversion and Management* 45.9 (2004): 1343-1356.

[33] Al-Farayedhi, A. A., Gandhidasan, P., & Al-Mutairi, M. A. "Evaluation of heat and mass transfer coefficients in a gauze-type structured packing air dehumidifier operating with liquid desiccant." *International Journal of Refrigeration* 25.3 (2002): 330-339.

[34] Liu, X. H., Chang, X. M., Xia, J. J., & Jiang, Y. "Performance analysis on the internally cooled dehumidifier using liquid desiccant." *Building and Environment* 44.2 (2009): 299-308.

[35] Yin, Y., Zhang, X., Wang, G., & Luo, L. "Experimental study on a new internally cooled/heated dehumidifier/regenerator of liquid desiccant systems." *International Journal of Refrigeration* 31.5 (2008): 857-866.

[36] Wang, Z., Zhang, X., & Li, Z. "Investigation on the coupled heat and mass transfer process between extremely high humidity air and liquid desiccant in the counter-flow adiabatic packed tower." *International Journal of Heat and Mass Transfer* 110 (2017): 898-907.

[37] Jain, S., Tripathi, S., & Das, R. S. "Experimental performance of a liquid desiccant dehumidification system under tropical climates." *Energy Conversion and Management* 52.6 (2011): 2461-2466.

[38] Luo, Y., Yang, H., Lu, L., & Qi, R. "A review of the mathematical models for predicting the heat and mass transfer process in the liquid desiccant dehumidifier." *Renewable and Sustainable Energy Reviews* 31 (2014): 587-599.

[39] Jeong, S., Garimella, S. "Falling-film and droplet mode heat and mass transfer in a horizontal tube LiBr/water absorber." *International Journal of Heat and Mass Transfer*, 45.7 (2002): 1445-1458.

[40] Abdul-Wahab, S. A., Abu-Arabi, M. K., & Zurigat, Y. H. "Effect of structured packing density on performance of air dehumidifier." *Energy Conversion and Management* 45.15-16 (2004): 2539-2552.

[41] Bonn, D., Eggers, J., Indekeu, J., Meunier, J., & Rolley, E. "Wetting and spreading." *Review of Modern Physics* 81.2 (2009):739-805.

[42] Liu, C., Bonaccurso, E., & Butt, H. J. "Evaporation of sessile water/ethanol drops in a controlled environment." *Physical Chemistry Chemical Physics* 10.47 (2008): 7150-7157.

[43] Qu, X., Davis, E.J., Swanson, B.D., "Non-isothermal droplet evaporation and condensation in the near-continuum regime", *Journal of Aerosol Science* 32.11 (2001): 1315-1339.

[44] Kita, Y., Okauchi, Y., Fukatani, Y., Orejon, D., Kohno, M., Takata, Y., Sefiane, K. "Quantifying vapor transfer into evaporating ethanol drops in humid atmosphere." *Physical Chemistry Chemical Physics* 20 (2018): 19430-19440.

[45] Nath, S., Bisbano, C. E., Yue, P., Boreyko, J. "Duelling dry zones around hygroscopic droplets." *Journal of Fluid Mechanics* 855 (2018): 601-620.

[46] Wimby, J. M., & Berntsson, T. S. "Viscosity and density of aqueous solutions of lithium bromide, lithium chloride, zinc bromide, calcium chloride and lithium nitrate. 1. Single salt solutions." *Journal of Chemical and Engineering Data* 39.1 (1994): 68-72.

View Article Online
DOI: 10.1039/C8CP04504F

[47] Hopkins, R. J., & Reid, J. P. "Evaporation of ethanol/water droplets: examining the temporal evolution of droplet size, composition and temperature." *The Journal of Physical Chemistry A* 109.35 (2005): 7923-7931.

[48] Christy, J.R.E., Hamamoto, Y., Sefiane, K. "Flow Transition within an Evaporating Binary Mixture Sessile Drop" *Physics Review Letters* 106 (2011): 205701.

[49] Dehaeck, S., Wylock, C., Colinet, P. "Evaporating cocktails" *Physics of Fluids* 21 (2009): 091108.

[50] Cussler, E. L. *Diffusion: Mass Transfer in Fluid Systems*. Cambridge University Press (Cambridge Series in Chemical Engineering), 2009.

[51] Lobo, V. M. M., Ribeiro, A. C. F., & Verissimo, L. M. P. "Diffusion coefficients in aqueous solutions of potassium chloride at high and low concentrations." *Journal of Molecular Liquids* 78.1-2 (1998): 139-149.

[52] Harned, H. S., & Levy, A. L. "The Differential Diffusion Coefficient of Calcium Chloride in Dilute Aqueous Solutions at 25°." *Journal of the American Chemical Society* 71.8 (1949): 2781-2783.

[53] Mitra, S., & Mitra, S. K. "Understanding the early regime of drop spreading." *Langmuir* 32.35 (2016): 8843-8848.

[54] Tanner, L. H. "The spreading of silicone oil drops on horizontal surfaces." *Journal of Physics D: Applied Physics* 12.9 (1979): 1473.

[55] Ruiter, R., Colinet, P., Brunet, P., Snoeijer, J.H., Gelderblom, H. "Contact line arrest in solidifying spreading drops" *Physical Review Fluids* 2 (2017): 043602.

[56] Shanahan, M. E. R. "Meniscus Shape and contact angle of a slightly deformed axisymmetric drop." *J. Phys. D: Appl. Phys.* 22 (1989): 1128-1135.

[57] Shanahan, M. E. R. "Simple Theory of "Stick-Slip" Wetting Hysteresis." *Langmuir* 11.3 (1995): 1041-1043.

[58] Shanahan, M. E. R. and Sefiane, K. "Contact Angle Wettability and Adhesion." *Taylor & Francis Group Koninklijke Brill NV Leiden The Netherlands by K. L. Mittal* 6 (2009): 19-32.

[59] Young, T. "An essay on the cohesion of fluids." *Philosophical Transactions of the Royal Society of London* 95 (1805): 65-87.

[60] Yao, W., Bjurstroem, H., & Setterwall, F. "Surface tension of lithium bromide solutions with heat-transfer additives." *Journal of Chemical and Engineering Data* 36.1 (1991): 96-98.

[61] Gittens, G. J. "Variation of surface tension of water with temperature." *Journal of Colloid and Interface Science* 30.3 (1969): 406-412.

[62] Tarasevich, Y.I. & Aksenenko, E.V. J. "Interaction of water molecules with hydrophilic and hydrophobic surfaces of colloid particles." *Journal of Water Chemistry and Technology* 37.5 (2015): 224-229.

[63] Bernett, Marianne K., and W. A. Zisman. "Effect of adsorbed water on wetting properties of borosilicate glass, quartz, and sapphire." *Journal of Colloid and Interface Science* 29.3 (1969): 413-423.

View Article Online
DOI: 10.1039/C8CP04504F

[64] Chengara, A., Nikolov, A. D., & Wasan, D. T. "Spreading of a water drop triggered by the surface tension gradient created by the localized addition of a surfactant." *Industrial & Engineering Chemistry Research* 46.10 (2007): 2987-2995.

[65] Bertozzi, A. L., Münch, A., Fanton, X., & Cazabat, A. M. "Contact line stability and "undercompressive shocks" in driven thin film flow." *Physical Review Letters* 81.23 (1998): 5169.

[66] Leger, L., Erman, M., Guinet-Picard, A. M., Ausserre, D., & Strazielle, C. "Precursor film profiles of spreading liquid drops." *Physical Review Letters* 60.23 (1988):2390-2393.

[67] Kavehpour, H. P., Ovryn, B., & McKinley, G. H. "Microscopic and Macroscopic Structure of the Precursor Layer in Spreading Viscous Drops." *Physical Review Letters* 91.19 (2003):196104.

[68] Colinet, P., Rednikov, A. "Chapter 4 – Precursor Films and Contact Line Microstructures" *Droplet Wetting and Evaporation*, Oxford (2015):31-56.

[69] Xu, H., Shirvanyants, D., Beers, K., Matyjaszewski, K., Rubinstein, M., & Sheiko, S. S. "Molecular motion in a spreading precursor film." *Physical Review Letters* 93.20 (2004): 206103.

[70] Hoang, A., & Kavehpour, H. P. "Dynamics of nanoscale precursor film near a moving contact line of spreading drops." *Physical Review Letters* 106.25 (2011):254501.

[71] Ghiradella, H., Radigan, W., & Frisch, H. L. "Electrical resistivity changes in spreading liquid films." *Journal of Colloid and Interface Science* 51.3 (1975): 522-526.

[72] Carré, A., Gastel, J. C., & Shanahan, M. E. "Viscoelastic effects in the spreading of liquids." *Nature* 379 (1996):432-434.

TOC

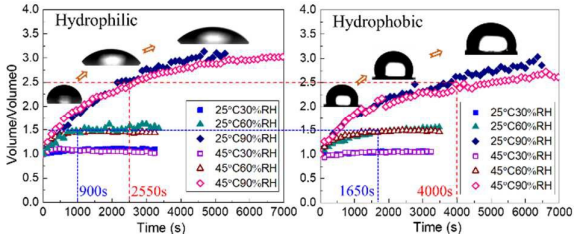

Mechanisms of droplet growth and spreading, related to surface wettability, are investigated during vapor absorption into hygroscopic lithium-bromide desiccant droplets.